*Article*

# Bone laser patterning to decipher cells organization

**Nicolas Touya[1*], Samy Al-Bourgol[2], Théo Désigaux[1], Olivia Kérourédan[1,3,4], Laura Gemini[2], Rainer Kling[2], Raphaël Devillard[1,3,4]**

[1] Univ. Bordeaux, INSERM, BIOTIS, U1026, F-33000 Bordeaux, France
[2] ALPhANOV, Rue François Mitterrand, 33400 Talence, France
[3] Faculty of Dentistry, University of Bordeaux, 146 rue Léo Saignat, Bordeaux 33076, France
[4] CHU de Bordeaux, Pôle de Médecine et Chirurgie bucco-dentaire, Place Amélie Raba Léon, Bordeaux 33076, France
* Correspondence: nicolas.touya@u-bordeaux.fr;

**Abstract:** Laser patterning of implant materials for bone tissue engineering purposes has shown to be a promising technique to control cell properties such as adhesion or differentiation, resulting in an enhanced osteointegration. However, the perspective of patterning the bone tissue side interface to generate microstructure effects has never been investigated. In the present study, three different laser-generated patterns were machined on the bone surface with the aim to identify the best surface morphology compatible with osteogenic-related cells recolonization. The laser patterned bone tissue was characterized by electron scanning microscopy and confocal microscopy in order to obtain a comprehensive picture of the bone surface morphology. Cortical bone patterning impact upon cell compatibility and cytoskeleton rearrangement to the patterned surfaces was performed with Stromal Cells from Apical Papilla (SCAPs). Results indicated that laser machining had no detrimental effect upon consecutively seeded cells metabolism. Orientation assays revealed that surface patterning characterized by larger hatch distances was correlated with a higher cell cytoskeletal conformation to the laser-machined patterns. For the first time, to our knowledge, bone is considered and assessed here as a potentially engineered-improvable biological interface. Further studies shall focus on in vivo implications of this direct patterning.

**Keywords:** tissue engineering; bone; laser; femtosecond; patterning; direct;

## 1. Introduction

In the last years, surface modification has become a critical aspect of tissue engineering [1,2] to improve osteointegration of implants and influence cell fate [3]. Investigations were led over various synthetic materials designed to substitute bone tissue as prostheses, such as ceramic [4–6], metal [7–10], and polymers [11]. An in vivo study outlined the strategical interest of modifying the topography of implants with laser, by showing a stronger bone-to-implant bond [12]. Femtosecond (fs) lasers particularly allow the biological response tailoring of a surface morphology by controlling surface pattern geometry down to 100s-nm scale [13–15], thanks to their unique characteristic. Indeed, Ultra Short Pulses (USP) allow a quasi-non-thermal interaction with materials and the generation of interference-based physical phenomena [16]. For example, Carvalho *et al.* reported an increased metabolic activity of MC3T3 (osteoblastic-related cells) cultured on Alumina toughened Zirconia (ATZ) where grid-structures or groove-like structures were generated upon fs laser machining; Gnilitskyi *et al.* demonstrated a higher ratio of HDFa (fibroblast cells) growth on both laser-nanostructured titanium alloy and zirconium, showing the predominant role of surface morphology over the material type for these types of biological response; A similar result was achieved by Lee *et al.*, where a variation of Saos-2 (osteoblastic-related cells) response and surface biocompatibility was observed down to a few 100s-nm pattern size difference.

 doi:10.20944/preprints202212.0074.v1

Due to these unique characteristics, these types of laser sources are currently considered in the frame of ablation of bone tissue for applications in surgeries where it is fundamental (i) to preserve the healthy status of the tissue after treatment to improve its biological response, such as implant integration, and (ii) to reach high-resolution modification of the tissue, as for instance in specific maxillofacial surgery approaches. A few reports showed the possibility to avoid detrimental thermal effect on bone tissue after UPS laser ablation, cutting and drilling [17,18]. Detrimental effects linked to thermal accumulation, such as the presence of microparticles of melted tissue and calcined tissue, were reported to be visible on the bone tissue down to the nanosecond (ns) regime of laser-tissue interaction and to become negligible for laser pulse duration below a few ps and optimised laser process parameters [19].

In this context, while a very few reports on laser patterning of synthetic hydroxyapatite are available [20], to our knowledge, no reports are available in the literature dedicated to direct bone patterning by fs laser. This new aspect of tissue interface could promote osteointegration of grafts, and/or synergize with superior osteointegration of laser-treated implants. In this study, patterning bone to potentialize current and future biomedical applications was evaluated in an *in vitro* model, as a first step towards a possible development to next-generation strategies for the engineering of bone/implant interface.

## 2. Materials and Methods

### *2.1. Bone tissue supply*

Porcine femurs were collected from the same place and labelled with the age and sex of the animals. All animals from which those femurs were retrieved were intended to human food consumption, in respect of French and European regulations regarding breeding, slaughter, and hygiene-sanitation in meat industry.

The bones were stored after reception in a freezer at a temperature of about -20 °C. To prepare the bone tissue for the laser treatment, it was left defrosting at room temperature in a laminar air-flow protection system (Thermo Scientific HERAsafe KS12, France). The proximal and distal epiphysis, as well as the metaphysis parts were then mechanically removed in order to obtain a clean cut of the diaphysis. Soft and fatty tissue, including bone marrow, were removed by scalpel. Finally, several samples (approx. 1x1x0.5 cm) were obtained (Figure 1) from the diaphysis by mechanical cutting using a diamond blade for easier handling during the processing and characterization steps. All bone samples were sanded by a mechanical sanding system (EcoMet 300, Buehler, USA). Their thickness, width and height were measured after sanding to ensure that all sample dimensions were homogeneous. In order to sterilize the tissue before laser processing, all samples were soaked in successive ethanol baths (24h at 90% concentration and 4h at 100% concentration, room temperature).

### *2.2. Laser-assisted patterning of bone*

A Satsuma HP2 (Amplitude, Talence, France) was employed for all tests. The laser ran at a central wavelength of 1030 nm with a maximum average power of 40 W and pulse duration of about 350 fs. The laser beam was firstly sent through a half-wave plate coupled with a polarising cube for a fine control of the laser pulse energy and then through a telescope system to adjust the beam size before the focusing optics (Figure 1). The laser beam was deflected on the sample by a galvanotric scanning head (Scan*CUBE*, ScanLAB, Munich, Germany) and focused by a 100mm f-theta lens on the sample surface. For all tests the following process parameters were kept constant: laser repetition rate of 500 kHz, average power of 5.28 W and scanning speed of 4 m/s. The selection of the processing parameters was done according to results from the same group [16], which showed that in the selected process window it was possible to ablate the bone tissue without important thermal damage. A cross-hatch pattern was generated on the sample surface with hatch

Preprints (www.preprints.org) | NOT PEER-REVIEWED | Posted: 5 December 2022 doi:10.20944/preprints202212.0074.v1

distance defined as the distance between two consecutive lines. Three different values of hatch distance were selected: h=25; 45; 65 µm. In order to achieve reliable and reproductible ablation depth values, the cross-hatch pattern was repeated 10 times for each tests. An aspiration system and an air-knife were employed to efficiently remove the bone debris and particules during laser ablation. The samples were placed on motorised stages for automated positioning before laser processing.

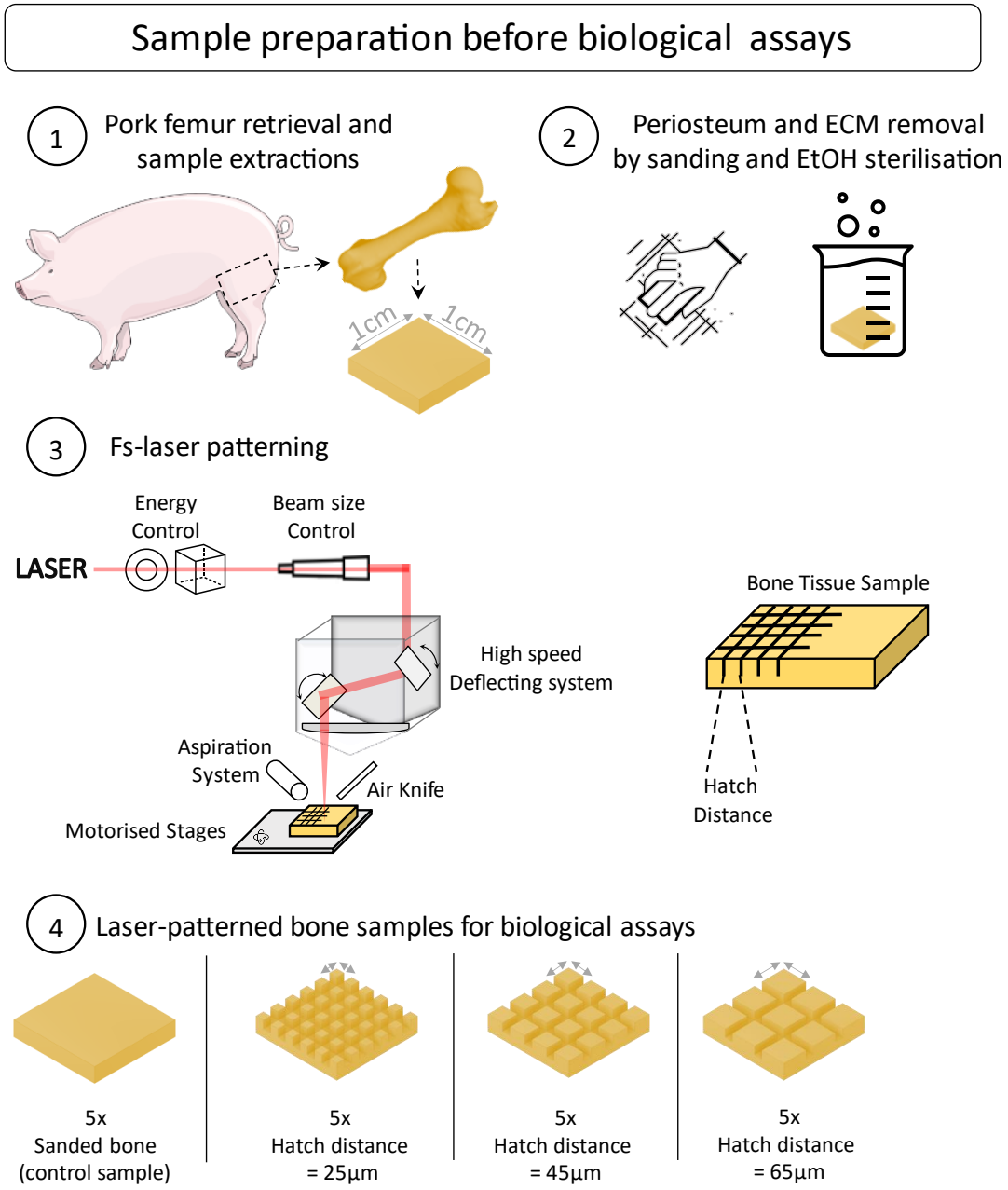


**Figure 1.** *Illustrated experimental approach and protocols for preparation of bone sample preparation before biological assays.*

Profilometric assays were performed with software Confomap v8 according to methods described in ISO 5436."

*2.3. Cell culture*

The human Stromal Cells from Apical Papilla (SCAPs) used for the hereby experiments were taken from a batch of cells already characterized [21]. The cells were amplified and cultured under 21%$O_2$. Briefly, cells were derived from germs of third molars, obtained from young patients at the *Service de Médecine bucco dentaire du Centre Hospitalier*

 doi:10.20944/preprints202212.0074.v1

*Universitaire de Bordeaux*. All experimental protocols were led following guidelines and regulations, under Ministerial approbation regarding french law ('DC-2008-412'; *convention INSERM-CHU de Bordeaux*). All patients gave their explicit consent to have their samples used for research purposes. If patients were under majority status regarding age, an additional consent from a parent and/or legal guardian was requested. Samples were treated anonymously. Freshly extracted teeth were placed in Minimum Essential Medium Alpha ($\alpha$-MEM, Gibco, Paisley, Scotland, UK) supplemented with 20% FBS and penicillin (100 U $ml^{-1}$)/streptomycin (100µg.$ml^{-1}$) (Life Technologies, SAS). Cells were extracted according to previously described method [22]. Dental apical papillae were digested in a mixture of 3mg.$ml^{-1}$ collagenase (Sigma-Aldrich) and 4 mg.$ml^{-1}$ dispase (Sigma-Aldrich) for 1 h at 37°C. The obtained suspension was sifted through a 40µm hole-size nylon sieve (BD Biosciences, France) and cells were then seeded in a 75$cm^2$ culture flask (37°C, 5% $CO_2$). Non-adherent cells were removed after 2 days, and the medium was changed thrice a week until cells reached 95% confluence. All SCAPs were amplified or cultured in tissue culture flasks in $\alpha$-MEM supplemented with 10% FBS, in a controlled atmosphere (5% $CO_2$, 95% Relative Humidity, 37°C). All cells were cultured and used for experimentations with a maximum passage number under 5.

### *2.4. Cells preparation*

Cells were detached from the polystyrene tissue culture surface with a solution of trypsin-EDTA (0.05% 1X Gibco, UK). Cells were suspended in their respective culture media. The cell suspension concentration was adjusted to 10 million cells.$ml^{-1}$, according to previously described protocol [23].

### *2.5. Metabolic assay*

After being washed in culture medium, all samples were placed over 2% w/v agarose coated wells. An identical number of non-labeled cells (2000 cells.$mm^{-2}$) were seeded over laser-machined areas and over non-machined samples. As control, some cells were seeded over uncoated wells. Media were renewed every two days, and observations were realized at days 1, 3, 5 and 7. Briefly, AlamarBlue™ [24] (0.1mg.$ml^{-1}$, Sigma-Aldrich, France) was diluted at 1:15 (v/v) in standard culture medium and placed with cells for 2h at 37°C. Supernatants were retrieved and transferred to a microplate while wells containing cells were rinsed, then refilled with standard culture medium and placed back to the incubator. Plate reading was performed with Varioskan Lux (Thermoscientific, US) spectrophotometer ($\lambda_{ex}$ 530nm and $\lambda_{em}$ 590nm).

### *2.6. Qualitative observations by Confocal Imaging and Scanning Electron Microscopy*

After the last metabolic assay on day 7, all the samples were rinsed in phosphate-buffered saline (PBS) and fixed in paraformaldehyde (4% w/v) overnight. Surfaces where cells were seeded were covered by permeabilization mix (BSA 2% (w/v), Triton 0.1% v/v) for 2h at 37°C. A staining mix composed of DAPI (0.1% v/v) and Alexa546-conjugated phalloidin (0.5% v/v) in permeabilization mix, was then applied for 2h at 37°C. All samples were rinsed mulitple times in PBS solution before confocal microscopy acquisition (Leica TCS SPE). ImageJ [25] and Imaris (Oxford Instruments plc.) softwares were used to perform the qualitative analysis of the acquisitions.

Samples were dried in consecutives ethanol baths (30%, 50%, 70%, 90% and 99%) with 1h soaking steps, and coated with gold with a sputter coater (EMSCOPE SC500, Elexience, France) before SEM (TM4000+ Hitachi, Japan) observations.

### *2.7. Cytoskeleton orientation assays*

The For quantitative analysis of cytoskeleton rearrangement, the Fiji plugin Directionnality tool (freely available on GitHub https://github.com/fiji/Directionality) was used. Firstly, hyperstacks of height-through acquisitions were performed. Sample matrix opacity-mediated autofluorescence was found to be equal in all conditions observed.

 doi:10.20944/preprints202212.0074.v1

All pictures were manually aligned according to the laser-carved patterns, so the trenches would be parallel (0° and 180°) and perpendicular (90°) to the Fast Fourier Transform (FFT) plan.

As SCAPs physiologically self-organize in spindle-shape with narrowing space between cells as the population grows, an increase in signal was expected to be reached at a certain angle. Control samples were then oriented in respect to this physiological feature, at 0° and 180° with respect to the FFT plan. To refine the orientation results, 180 steps of FFT were performed from -45° to 134°.

All results were then gathered and analyzed through GraphPad Prism version 8.0.0 software (GraphPad Software, San Diego, California USA) to generate the FFT heatmaps. Circular histograms frequency plots (with frequency proportional to the area of each bar) were obtained through the adaptation of an opensource code from matplotlib.org (version used for this article available upon request and free of use).

### *2.8. Statistical analysis*

All tests were performed using GraphPad Prism version 8.0.0 software (GraphPad Software, San Diego, California USA). Non-parametric tests were selected when normality test failed, or when the sample size was unsufficient. H0 hypothesis was rejected when p-value < 0.05.

Preprints (www.preprints.org) | NOT PEER-REVIEWED | Posted: 5 December 2022 doi:10.20944/preprints202212.0074.v1

## 3. Results

### *3.1. Systematic review following PRISMA guidelines*

a

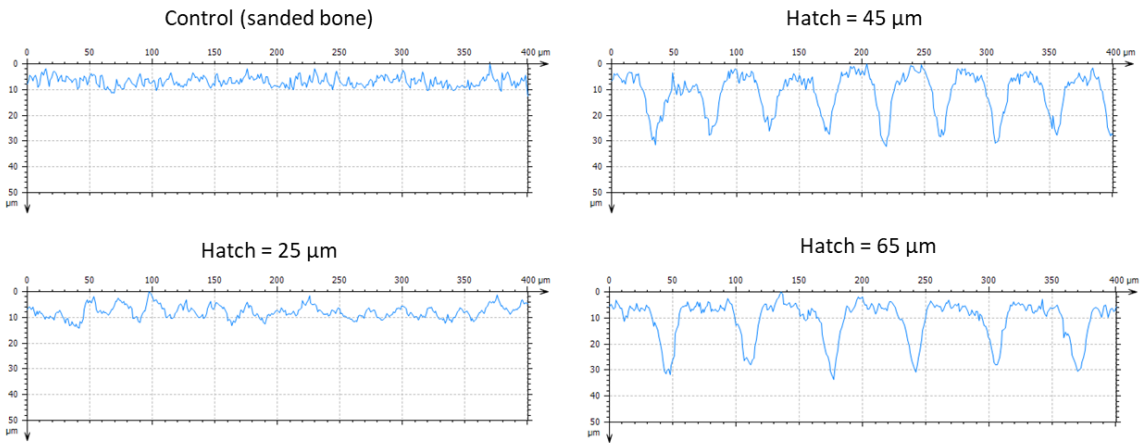


b

| Condition | Measured hatch (µm) ± Std dev | Ablation width (µm) ± Std dev | Ablation Depth (µm) ± Std dev | Ablated area (%) |
|---|---|---|---|---|
| Control † | N/A | 5.37 ± 1.8 | 4.35 ± 0.99 | N/A |
| H25 | 25.61 ± 4.8 | 8.14 ± 2.7 | 4.46 ± 1.1 | 36.6 |
| H45 | 45.52 ± 1.9 | 8.36 ± 1.7 | 20.06 ± 2.3 | 26.2 |
| H65 | 63.95 ± 1.9 | 8.5 ± 1.1 | 21.5 ± 1.1 | 20.7 |

c

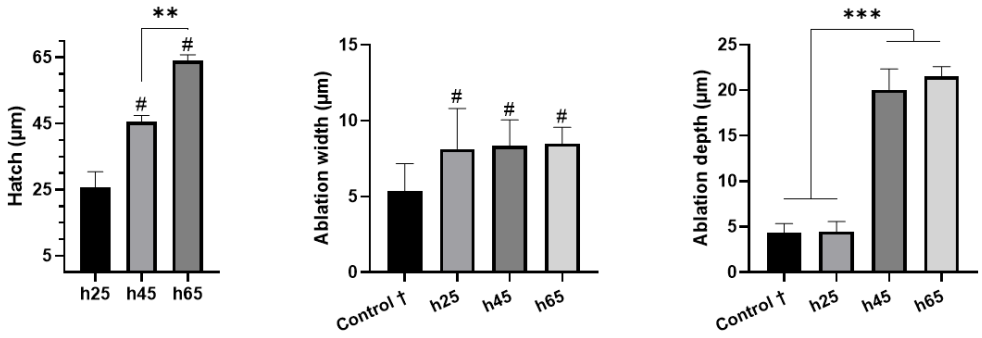


**Figure 2.** *Profilometric analysis of control (sanded bone) and laser-patterned samples. Examples of each condition surface morphology (a) acquired with Confomap ST 8.2 software. Descriptive statistics (b) and statistical tests (c) of patterning physical parameters (Kruskal-Wallis, * p<0.05, ** p<0.01, ***p<0.001, # = *** compared to leftmost bar. N=3, n ≥ 12). †: controls were not patterned with laser. Numbers are displayed as intrinsic sample surface morphology.*

Descriptive statistics of all obtained measurements were also reported in Figure 2. For the profiles obtained on samples treated with hatch distance of 25 µm, microroughness was adjusted by applying a band-pass filtering with cut-off wavelenght of 5 µm in order to have more reliable data. It is important to underline that control samples (sanded bones) were used as reference, and values are displayed to depict the intrinsic surface morphology post-sanding. Measured hatch were respectful to the experimental procedure with high reproducibility. Ablation width was found to be constant regardless of the hatch employed. However, ablation depth result highlighted that a 25µm hatching was ablating a large area of bone. As a result, the surface morphology became similar to control. With the increase of the hatch, ablation depth was found to generate around 21µm deep pattern through cortical bone.

Preprints (www.preprints.org) | NOT PEER-REVIEWED | Posted: 5 December 2022 doi:10.20944/preprints202212.0074.v1

*3.2. Laser machining impact over recolonizing cells survival*

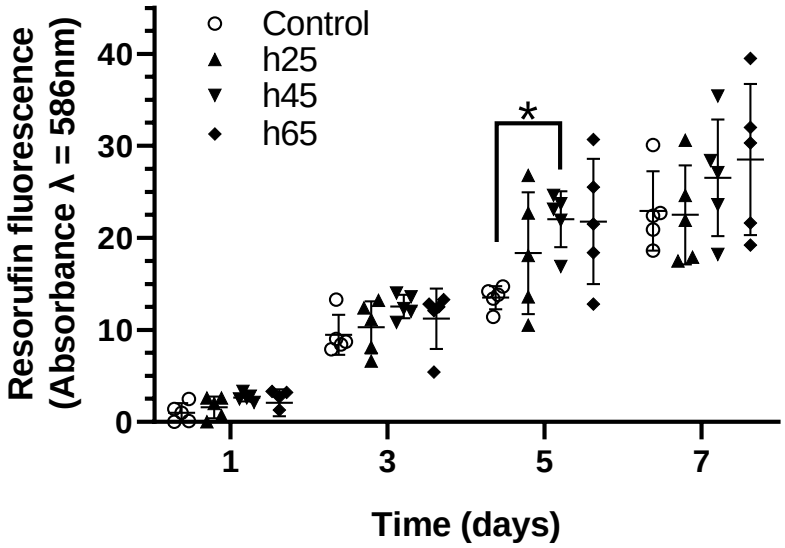


**Figure 3.** *Metabolic activity of SCAPs seeded over different laser-treated samples. 2000 cells.mm$^{-2}$ were seeded at day 0, and measurements were performed on days 1, 3, 5 and 7. Normalized resorufin measured absorbance shows cell viability and growth indirectly via NADH dehydrogenase activity through time. n=5, Kruskal-Wallis test *: p<0.05*

The levels of resazurin reduction in SCAPs cultured over laser patterned bones, regardless of the patterns geometry, were similar to the behaviour of SCAPs cultured on control samples (Figure 3). Through time, SCAPs increased their metabolic activity. In all experiment led, absorbances from 25µm hatch distance were observed to be close to control, while a tendency of higher absorbances was noticed from 45µm and 65µm hatch distances. At day 5, fluorescence signal from samples patterned with 45µm hatch distance was found to be significantly higher than control. Altogether, these results suggest that laser patterning of bone tissue as cell deposition pre-treatment is cytocompatible and suitable for SCAPs metabolism.

*3.3. Laser machining impact over cell orientation*

Confocal microscopy imaging of cells after 7 days of culture (Figure 4) gave a first qualitative information on cell morphology with respect to the specific laser-generated patterns.

Preprints (www.preprints.org) | NOT PEER-REVIEWED | Posted: 5 December 2022 doi:10.20944/preprints202212.0074.v1

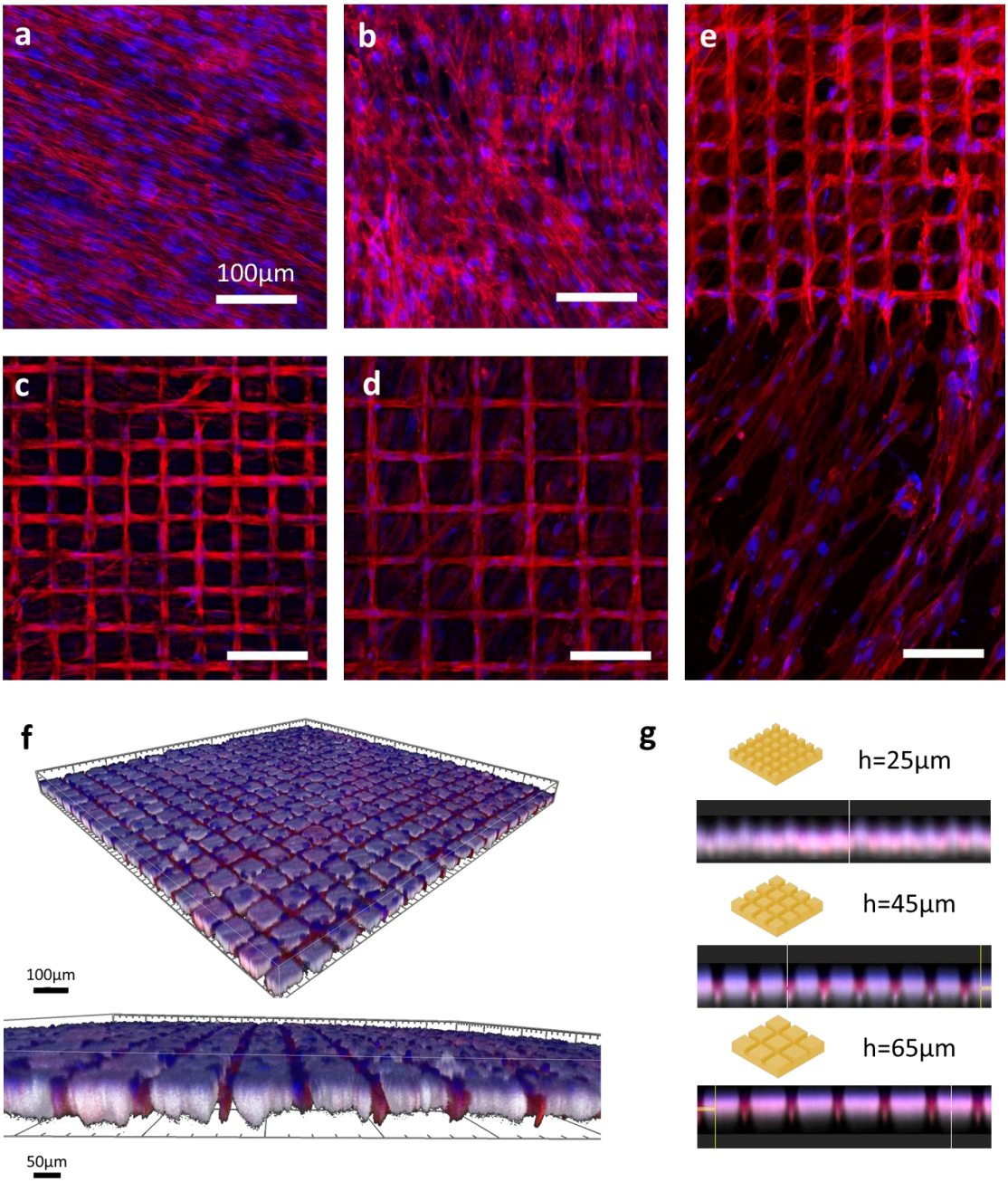


**Figure 4.** *Confocal Microscopy imaging of SCAPs seeded over laser-patterned bones. F-actin (red) and nucleus (blue) structures were respectively stained by Alexa 546-Phalloidin and DAPI. Images were captured on confocal Leica TCS SPE microscope and assembled on ImageJ software. Images represent control sample (a), and samples patterned with hatch distances of 25µm (b), 45µm (c) and 65µm (d). The right-sided panel (e) shows the edge zone between the laser-patterned area and untreated bone. Unspecified scale bars = 100 µm. Lower panels depict 3D reconstruction of confocal z stacks acquisitions with illustration of sample with hatch distance of 65µm (f) and mean orthogonal views (g) of samples with 25, 45 and 65µm hatch distances*

Cells seeded over control samples (Figure 4a) had a very stretched, spindle shape. On samples patterned with a 25µm hatch distance (Figure 4b), cells showed a less self-organised arrangement yet started to visually respect a grid-like pattern, especially with the aligned aspect of nuclei distribution. However, a remarkable difference was observable (Figure 4e) from cells seeded over samples patterned with larger hatch distance; indeed, for samples with 45 and 65µm hatch distance (respectively Figure 4c and 4d), cells were mostly contained within the ablated pattern, even though actin filaments and some nuclei could be observed on area associated to untreated areas. 3D reconstructions (Figure 4f)

Preprints (www.preprints.org) | NOT PEER-REVIEWED | Posted: 5 December 2022 doi:10.20944/preprints202212.0074.v1

allowed to observe cell behaviour with a depeer insight, and highlighted the autofluorescence of bone imaged with UV wavelenghts, merging with nuclei signals. Looking at sideviews of 3D reconstructions (Figure 4g), higher intensities of actin staining were found within the cavities created by laser ablation, except for samples patterned with 25µm, where the signal was diffused. These observations were consistent with those made with the 2D stacks.

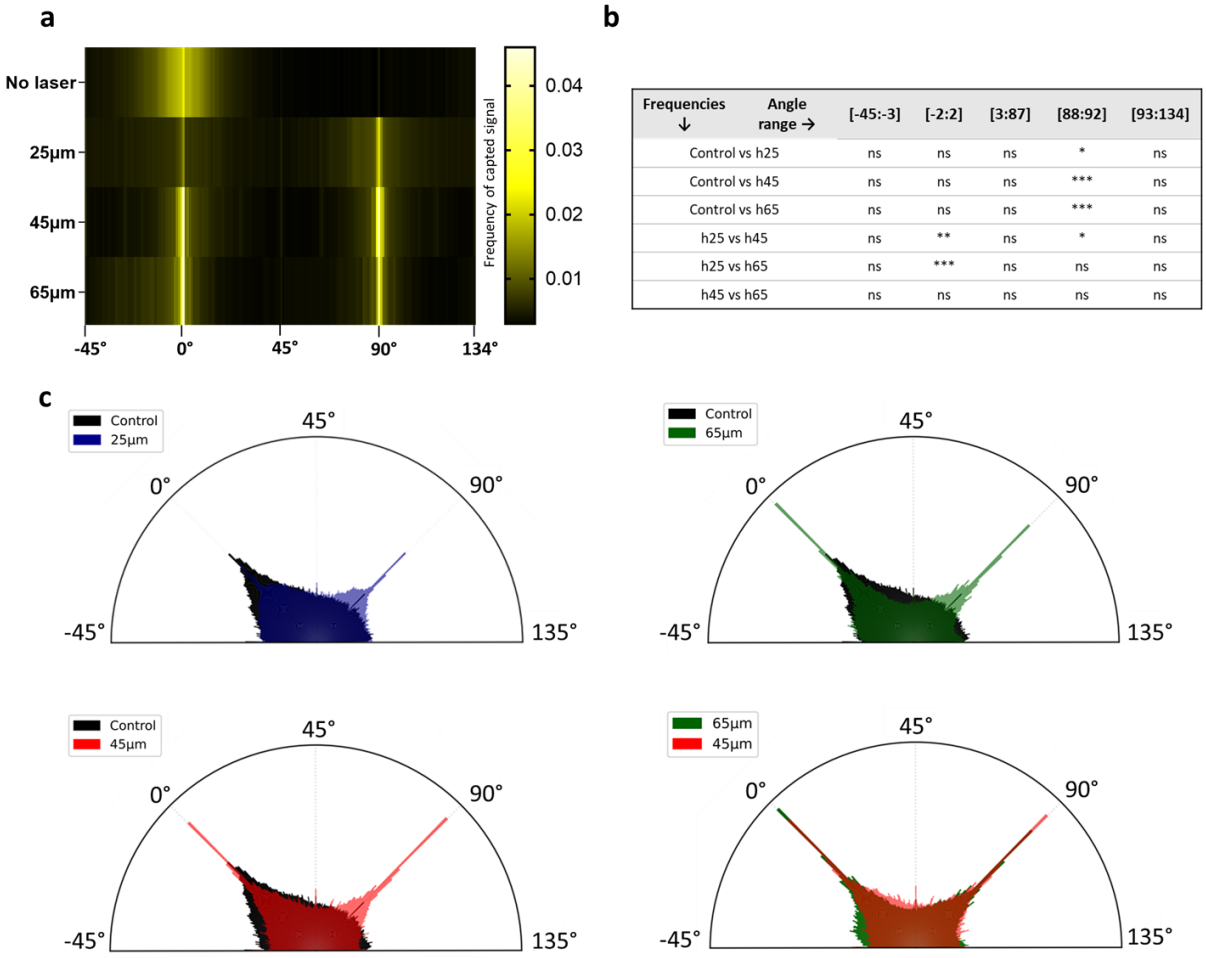


| Frequencies ↓ / Angle range → | [-45:-3] | [-2:2] | [3:87] | [88:92] | [93:134] |
|---|---|---|---|---|---|
| Control vs h25 | ns | ns | ns | * | ns |
| Control vs h45 | ns | ns | ns | *** | ns |
| Control vs h65 | ns | ns | ns | *** | ns |
| h25 vs h45 | ns | ** | ns | * | ns |
| h25 vs h65 | ns | *** | ns | ns | ns |
| h45 vs h65 | ns | ns | ns | ns | ns |

**Figure 5.** *Cell alignment after seeding over laser-patterned samples. Fast Fourier Transform heat map (above) highlights the influence of laser patterning on cell cytoskeletal arrangement, with higher frequencies of aligned cells at 0 and 90°, consistent with the pattern's orientations. Statistical tests were performed over means of angle ranges, with 5° range centered at 0° and 90°, and rest of angles gathering 95% of lowest values (Kruskal-Wallis, * p<0.05, ** p<0.01, ***p<0.001, ns = not significative, n=5). Cumulated frequency plots (below) (proportional to area of each bar) reveal that frequencies associated with 45 and 65µm samples presented overall lower dispersion, and higher frequencies at 0 and 90° angles. Control sample was displayed with an opacity of 100% while all other conditions had a 50% opacity to be stackable.*

Actin filaments orientation analyses were performed by FFT analyse of corresponding channel acquired by confocal microscopy. The retrieved data were analyzed and translated graphically with a heat map (Figure 5a) and frequency plots. On the heat maps, frequencies are proportionnal to the intensity of signal retrieved for each angle. A high frequency hence means a lot of signal from actin filaments. The more cells aligned with a given angle, the strongest the signal, and the higher the frequency obtained. Heat maps showed that, in absence of laser patterning, cells are preferentially oriented in a single range of angles with a single area of rise in frequencies. The laser patterning, being vertical and horizontal, induced two peaks of frequencies, regardless of the hatch size. However, significant differences were observed (Figure 5b) in frequencies between 25µm and the other hatch sizes around 0°. Around 90°, h25 vs h45 mean frequencies were found to be

Preprints (www.preprints.org) | NOT PEER-REVIEWED | Posted: 5 December 2022 doi:10.20944/preprints202212.0074.v1

significantly different, and frequencies from all test conditions were significantly different from control.

The frequency plots (Figure 5c) were generated based on the same data. The areas of each bar are proportionnal to the intensity of signal for each angle. While the heat map highlighted the effect of the patterns on dictating cell adhesion to a defined area, the frequency plots mainly outlined that increasing the hatch distance of the laser-generated pattern resulted in a decrease of the frequencies. Frequencies detected outside the 0° and 90° angles could be assimilated to cells that did not align to the laser-generated pattern: controls and 25µm patterned samples were associated to homogeneous dispersion and highest frequencies off 0 and 90° angles. By increasing hatch (45 and 65µm), frequencies lowered in out-of-interest ranges. Yet, these observations were not found to be significative.

Altogether, these results were highly consistent with qualitative results aforementioned: cells are mostly aligned with laser-generated patterns, especially regarding superior hatch distances of 45 and 65µm.

### 3.4. *Laser patterning impact over cell adhesion*

After confocal imaging, samples were observed with SEM (Figure 6).

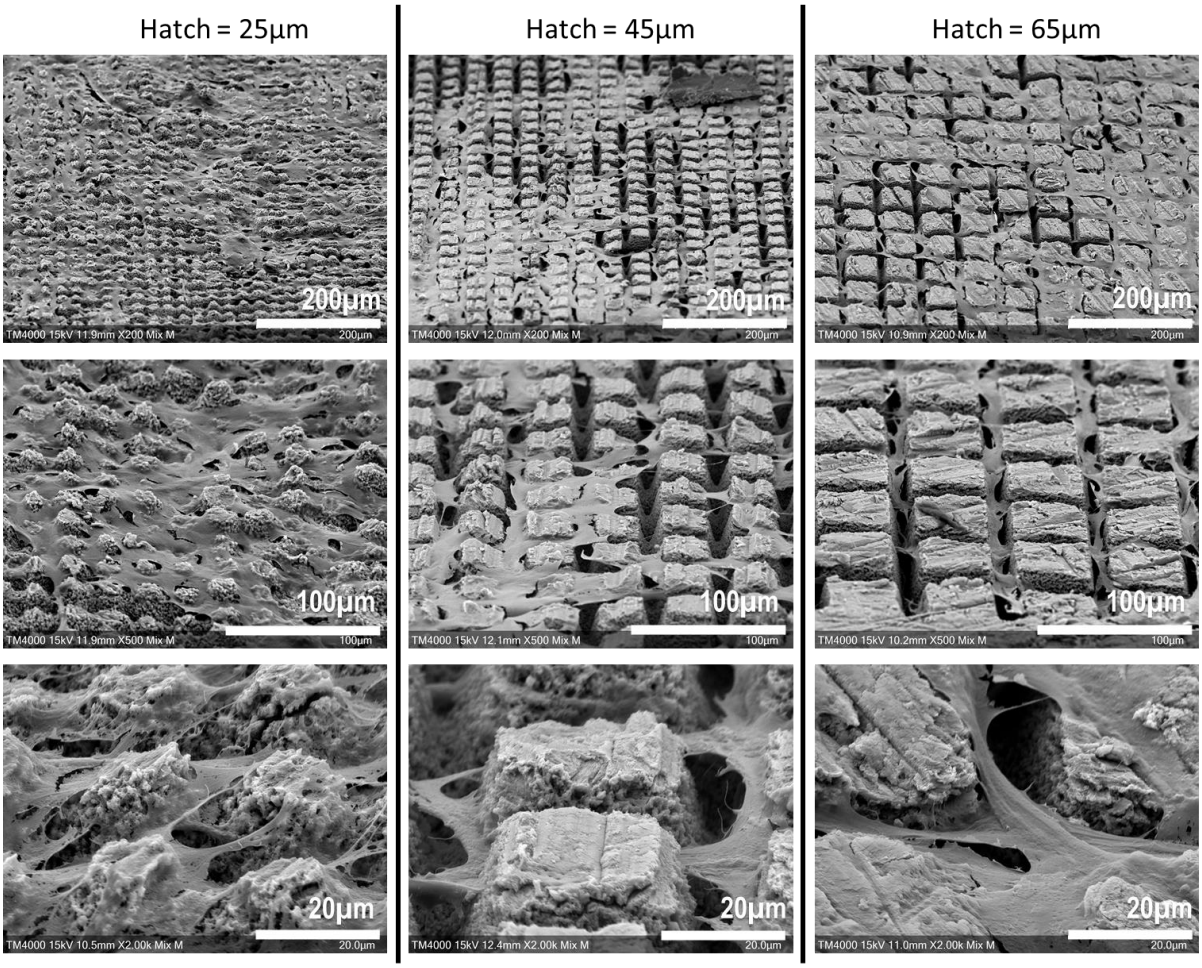


**Figure 6.** *Scanning Electron Microscopy imaging of SCAPs seeded over laser-machined bones. With higher magnifications, cells appear to adhere to the upper side of machined patterns and not at the bottom of it, where laser hit the most bone surface.*

This qualitative assessment of cells behavior upon machined area revealed that cells seemed to mostly adhere to the upper side of machined patterns while the remaining

 doi:10.20944/preprints202212.0074.v1

space at the bottom of the carved patterns was left unoccupied. However, cells did not prefer adhering to the untreated surface and fitted to the carved patterns, consistently with the confocal microscopy acquisitions.

**4. Discussion**

The results presented in this work on laser processing of bone tissue demonstrated once again the unique ability of fs laser sources to obtain highly resolutive laser-matter interaction to laser-functionalise a biological tissue by precisely tayloring the patterning geometry.

The machining parameters were dictated by two main aspects : designing a fast and reproducible process, and creating a microtextured surface having an impact on the behavior of osteogenic-related cells.

Hatch sizes were chosen with consideration to physiological cell characteristics and behavior. Average circulating MSC cell sizes being comprised between 15 and 30µm [26], thus influence of hatch over cell seeding was investigated. A hatch of 25µm generating surface roughly similar to non-patterned bone, cell settlement was not expected to be much influenced, besides the direct effect of laser-induced matter removal. Hatch sizes of 45µm and 65µm were associated to the creation of deeper patterns through the cortical bone (about 20µm deep). It was hypothetized that cells would preferentially occupy spaces offering three dimensionnal anchoring possibilities. The diminution of carved area proportion within pattern area was expected either to force cells to maximally fill the carved trenches, or to create a cell layer above the pattern and secrete extracellular matrix to overcome the gaps between non-carved areas.

In the experiment led, a depth limit ablation was found to be around 20 µm regardless of the hatch size, a quite common effect in fs laser ablation and could be linked to partial absorption or shielding of the incoming laser pulse from the laser generated plasma [27]. This depth limit allowed to maintain the difference between 45 and 65µm conditions solely due to the hatch distance discrimination. As seen with the profilometry assay, the ablated area had a conic form, tightening with increased ablation depth. The SEM observations of upperly-adherent cells within the pattern seems consistent with a narrowing available space at the bottom of the pattern, unreachable for large organites such as nucleus[28], which might force cells to remain be closer to the surface of the pattern.

Among the difficulties encountered, bone autofluorescence brought difficulty to properly image samples. Autofluorescence was corrected with the same tresholding for all samples to avoid any inter-acquisition bias. Post-acquisition additionnal tresholding to remove residual background noise was associated with partial loss of cell related information. Therefore, images were kept raw and treated under the same procedure for the Fast Fourier Transform. Still facing the difficulty to evaluate the cell viability through time, a metabolic assay was performed to compare cell activity, and give an indirect sight of cell proliferation through the different texturations evaluated.

SCAPs, a mesenchymal cell population comparable to bone-marrow derived MSCs [29,30], were used in this study as these progenitors are more likely to be recruited *in situ* rather than mature osteoblasts, and more representative of the diversity of osteoblastic cell populations. The impact of vascular-related cells such as endothelial cells should also be investigated in future work.

Laser ablation impact on bone tissue local gene expression profile was previously reported [31,32] and found to enhance osteogenesis compared to trepan ablation. However, in this case, all bones were sanded prior to laser texturation application to free the mineral matrix from organic ECM and periost. In future work, an increased interest should be brought to transcriptomics consequences of laser patterning.

Although many assays exist to quantify cell adhesion [33], the limitations of working with a thick and opaque material with such scale of texturation constituted an obstacle for

 doi:10.20944/preprints202212.0074.v1

all known standard techniques. As the stated ambition is the improvement of bone-material interface strength and quality, further work should be conducted *in vivo*, inspired by the quantitative assessment of osteointegration of Hallgren *et al.* [12] and performing histological investigations to investigate the physiological response of laser texturation.

The difficulty to adjust laser technology from benchside to operating room is likely the largest hurdle to see its medical application, considering the high cost of a laser compared to other technologies such as drills or ultrasonication [34,35]. However, this technology is employed with an unprecedent resolution. Moreover, laser patterning could be coupled with laser-assisted bioprinting technology [36], combining the possibility to reshape bone and then precisely project elements of interests (drugs, antibiotics, cells, growth factors…) directly *in situ*, with the same workstation and a unique laser source.

Some work was conducted using deep learning to optimize the development of laser machining, predicting the outcome of skeletal stem cells arrangement according to the laser-machined pattern [37]. The rise of AI-based technologies could significantly improve future research, especially in finding optimum parameters regarding patterning design and biological consequences. Future *in vivo* investigations should be performed with patterns designed to drive cellular colonization with facilitated settlement of, for example, vascular network.

## 5. Conclusions

For the first time, laser technology was applied directly to texture cortical bone in a perspective of developing new bone-graft materials interface insights for bone tissue engineering. Results showed the high technological potential of femtosecond laser-based processing in tailoring laser-generated bone patterning, and its great cytocompatibility with mesenchymal-derived stromal cells. The different patterns investigated unveiled the possibility to dictate cell orientation. Laser patterning was demonstrated to constitute a great opportunity to develop new aspect of host tissue and graft material interface, and direct patterning of host tissue could be considered in future application of medical devices to enhance grafts.

**Author Contributions:** Conceptualization, RD; methodology, RD; software, LG; validation, OK, LG and RK; formal analysis, NT; investigation, NT.; resources, NT and OK; data curation, NT and TD; writing—original draft preparation, NT; writing—review and editing, RD; visualization, NT; supervision, RD; project administration, RD. All authors have read and agreed to the published version of the manuscript.

**Funding:** No funding was associated to this work.

**Data Availability Statement:** All data gathered for this article are available from the authors upon reasonable request.

**Conflicts of Interest:** The authors declare no conflict of interest in the design of the study; in the collection, analyses, or interpretation of data; in the writing of the manuscript; or in the decision to publish the results.

## References

1. Barfeie, A.; Wilson, J.; Rees, J. Implant Surface Characteristics and Their Effect on Osseointegration. *Br Dent J* **2015**, *218*, E9, doi:10.1038/sj.bdj.2015.171.
2. Kang, C.-W.; Fang, F.-Z. State of the Art of Bioimplants Manufacturing: Part II. *Adv. Manuf.* **2018**, *6*, 137–154, doi:10.1007/s40436-018-0218-9.
3. West-Livingston, L.N.; Park, J.; Lee, S.J.; Atala, A.; Yoo, J.J. The Role of the Microenvironment in Controlling the Fate of Bioprinted Stem Cells. *Chem. Rev.* **2020**, *120*, 11056–11092, doi:10.1021/acs.chemrev.0c00126.

4. Baino, F.; Montealegre, M.A.; Minguella-Canela, J.; Vitale-Brovarone, C. Laser Surface Texturing of Alumina/Zirconia Composite Ceramics for Potential Use in Hip Joint Prosthesis. *Coatings* **2019**, *9*, 369, doi:10.3390/coatings9060369.
5. Daskalova, A.; Lasgorceix, M.; Bliznakova, I.; Angelova, L.; Hocquet, S.; Leriche, A.; Trifonov, A.; Buchvarov, I. Ultra-Fast Laser Surface Texturing of $\upbeta$-Tricalcium Phosphate ($\upbeta$-TCP) Ceramics for Bone-Tissue Engineering Applications. *J. Phys.: Conf. Ser.* **2020**, *1492*, 012059, doi:10.1088/1742-6596/1492/1/012059.
6. Lasgorceix, M.; Ott, C.; Boilet, L.; Hocquet, S.; Leriche, A.; Asadian, M.; De Geyter, N.; Declercq, H.; Lardot, V.; Cambier, F. Micropatterning of Beta Tricalcium Phosphate Bioceramic Surfaces, by Femtosecond Laser, for Bone Marrow Stem Cells Behavior Assessment. *Materials Science and Engineering: C* **2019**, *95*, 371–380, doi:10.1016/j.msec.2018.03.004.
7. Olsson, R.; Powell, J.; Palmquist, A.; Brånemark, R.; Frostevarg, J.; Kaplan, A.F.H. Production of Osseointegrating (Bone Bonding) Surfaces on Titanium Screws by Laser Melt Disruption. *Journal of Laser Applications* **2018**, *30*, 042009, doi:10.2351/1.5078502.
8. Man, H.C.; Chiu, K.Y.; Guo, X. Laser Surface Micro-Drilling and Texturing of Metals for Improvement of Adhesion Joint Strength. *Applied Surface Science* **2010**, *256*, 3166–3169, doi:10.1016/j.apsusc.2009.11.092.
9. Coathup, M.J.; Blunn, G.W.; Mirhosseini, N.; Erskine, K.; Liu, Z.; Garrod, D.R.; Li, L. Controlled Laser Texturing of Titanium Results in Reliable Osteointegration. *J Orthop Res* **2017**, *35*, 820–828, doi:10.1002/jor.23340.
10. Ulerich, J.P.; Ionescu, L.C.; Chen, J.; Soboyejo, W.O.; Arnold, C.B. Modifications of Ti-6Al-4V Surfaces by Direct-Write Laser Machining of Linear Grooves. In Proceedings of the Photon Processing in Microelectronics and Photonics VI; SPIE, March 13 2007; Vol. 6458, pp. 307–316.
11. Nuutinen, T.; Silvennoinen, M.; Päiväsaari, K.; Vahimaa, P. Control of Cultured Human Cells with Femtosecond Laser Ablated Patterns on Steel and Plastic Surfaces. *Biomed Microdevices* **2013**, *15*, 279–288, doi:10.1007/s10544-012-9726-8.
12. Hallgren, C.; Reimers, H.; Chakarov, D.; Gold, J.; Wennerberg, A. An in Vivo Study of Bone Response to Implants Topographically Modified by Laser Micromachining. *Biomaterials* **2003**, *24*, 701–710, doi:10.1016/s0142-9612(02)00266-1.
13. Carvalho, A.; Grenho, L.; Fernandes, M.H.; Daskalova, A.; Trifonov, A.; Buchvarov, I.; Monteiro, F.J. Femtosecond Laser Microstructuring of Alumina Toughened Zirconia for Surface Functionalization of Dental Implants. *Ceramics International* **2020**, *46*, 1383–1389, doi:10.1016/j.ceramint.2019.09.101.
14. Gnilitskyi, I.; Pogorielov, M.; Viter, R.; Ferraria, A.M.; Carapeto, A.P.; Oleshko, O.; Orazi, L.; Mishchenko, O. Cell and Tissue Response to Nanotextured Ti6Al4V and Zr Implants Using High-Speed Femtosecond Laser-Induced Periodic Surface Structures. *Nanomedicine: Nanotechnology, Biology and Medicine* **2019**, *21*, 102036, doi:10.1016/j.nano.2019.102036.
15. Lee, B.E.J.; Exir, H.; Weck, A.; Grandfield, K. Characterization and Evaluation of Femtosecond Laser-Induced Sub-Micron Periodic Structures Generated on Titanium to Improve Osseointegration of Implants. *Applied Surface Science* **2018**, *441*, 1034–1042, doi:10.1016/j.apsusc.2018.02.119.
16. Gemini, L.; Al-Bourgol, S.; Machinet, G.; Bakkali, A.; Faucon, M.; Kling, R. Ablation of Bone Tissue by Femtosecond Laser: A Path to High-Resolution Bone Surgery. *Materials* **2021**, *14*, 2429, doi:10.3390/ma14092429.
17. Plötz, C.; Schelle, F.; Bourauel, C.; Frentzen, M.; Meister, J. Ablation of Porcine Bone Tissue with an Ultrashort Pulsed Laser (USPL) System. *Lasers Med Sci* **2015**, *30*, 977–983, doi:10.1007/s10103-014-1520-9.
18. Cangueiro, L.T.; Vilar, R.M.C. da S.; Rego, A.M.B. do; Muralha, V.S.F. Femtosecond Laser Ablation of Bovine Cortical Bone. *JBO* **2012**, *17*, 125005, doi:10.1117/1.JBO.17.12.125005.
19. Girard, B.; Yu, D.; Armstrong, M. r.; Wilson, B. c.; Clokie, C. m. l.; Miller, R.J.D. Effects of Femtosecond Laser Irradiation on Osseous Tissues. *Lasers in Surgery and Medicine* **2007**, *39*, 273–285, doi:10.1002/lsm.20466.

20. Um, S.-H.; Lee, J.; Song, I.-S.; Ok, M.-R.; Kim, Y.-C.; Han, H.-S.; Rhee, S.-H.; Jeon, H. Regulation of Cell Locomotion by Nanosecond-Laser-Induced Hydroxyapatite Patterning. *Bioactive Materials* **2021**, *6*, 3608–3619, doi:10.1016/j.bioactmat.2021.03.025.
21. Rémy, M.; Ferraro, F.; Le Salver, P.; Rey, S.; Genot, E.; Djavaheri-Mergny, M.; Thébaud, N.; Boiziau, C.; Boeuf, H. Isolation and Culture of Human Stem Cells from Apical Papilla under Low Oxygen Concentration Highlight Original Properties. *Cells* **2019**, *8*, E1485, doi:10.3390/cells8121485.
22. Sonoyama, W.; Liu, Y.; Yamaza, T.; Tuan, R.S.; Wang, S.; Shi, S.; Huang, G.T.-J. Characterization of the Apical Papilla and Its Residing Stem Cells from Human Immature Permanent Teeth: A Pilot Study. *J Endod* **2008**, *34*, 166–171, doi:10.1016/j.joen.2007.11.021.
23. Touya, N.; Devun, M.; Handschin, C.; Casenave, S.; Ahmed Omar, N.; Gaubert, A.; Dusserre, N.; De Oliveira, H.; Kérourédan, O.; Devillard, R. In Vitroandin Vivocharacterization of a Novel Tricalcium Silicate-Based Ink for Bone Regeneration Using Laser-Assisted Bioprinting. *Biofabrication* **2022**, *14*, doi:10.1088/1758-5090/ac584b.
24. Rampersad, S.N. Multiple Applications of Alamar Blue as an Indicator of Metabolic Function and Cellular Health in Cell Viability Bioassays. *Sensors (Basel)* **2012**, *12*, 12347–12360, doi:10.3390/s120912347.
25. Schneider, C.A.; Rasband, W.S.; Eliceiri, K.W. NIH Image to ImageJ: 25 Years of Image Analysis. *Nat Methods* **2012**, *9*, 671–675, doi:10.1038/nmeth.2089.
26. Khan, R.S.; Newsome, P.N. A Comparison of Phenotypic and Functional Properties of Mesenchymal Stromal Cells and Multipotent Adult Progenitor Cells. *Frontiers in Immunology* **2019**, *10*.
27. Zhang, H.; van Oosten, D.; Krol, D.M.; Dijkhuis, J.I. Saturation Effects in Femtosecond Laser Ablation of Silicon-on-Insulator. *Appl. Phys. Lett.* **2011**, *99*, 231108, doi:10.1063/1.3666423.
28. Webster, M.; Witkin, K.L.; Cohen-Fix, O. Sizing up the Nucleus: Nuclear Shape, Size and Nuclear-Envelope Assembly. *J Cell Sci* **2009**, *122*, 1477–1486, doi:10.1242/jcs.037333.
29. Shi, S.; Robey, P.G.; Gronthos, S. Comparison of Human Dental Pulp and Bone Marrow Stromal Stem Cells by CDNA Microarray Analysis. *Bone* **2001**, *29*, 532–539, doi:10.1016/s8756-3282(01)00612-3.
30. Yamada, Y.; Fujimoto, A.; Ito, A.; Yoshimi, R.; Ueda, M. Cluster Analysis and Gene Expression Profiles: A CDNA Microarray System-Based Comparison between Human Dental Pulp Stem Cells (HDPSCs) and Human Mesenchymal Stem Cells (HMSCs) for Tissue Engineering Cell Therapy. *Biomaterials* **2006**, *27*, 3766–3781, doi:10.1016/j.biomaterials.2006.02.009.
31. Shimohira, T.; Katagiri, S.; Ohsugi, Y.; Hirota, T.; Hatasa, M.; Mizutani, K.; Watanabe, K.; Niimi, H.; Iwata, T.; Aoki, A. Comprehensive and Sequential Gene Expression Analysis of Bone Healing Process Following Er:YAG Laser Ablation. *Photobiomodul Photomed Laser Surg* **2021**, *39*, 100–112, doi:10.1089/photob.2020.4833.
32. Ohsugi, Y.; Aoki, A.; Mizutani, K.; Katagiri, S.; Komaki, M.; Noda, M.; Takagi, T.; Kakizaki, S.; Meinzer, W.; Izumi, Y. Evaluation of Bone Healing Following Er:YAG Laser Ablation in Rat Calvaria Compared with Bur Drilling. *Journal of Biophotonics* **2019**, *12*, e201800245, doi:10.1002/jbio.201800245.
33. Khalili, A.A.; Ahmad, M.R. A Review of Cell Adhesion Studies for Biomedical and Biological Applications. *Int J Mol Sci* **2015**, *16*, 18149–18184, doi:10.3390/ijms160818149.
34. Troedhan, A.; Mahmoud, Z.T.; Wainwright, M.; Khamis, M.M.; Troedhan, A.; Mahmoud, Z.T.; Wainwright, M.; Khamis, M.M. Cutting Bone with Drills, Burs, Lasers and Piezotomes: A Comprehensive Systematic Review and Recommendations for the Clinician. *International Journal of Oral and Craniofacial Science* **2017**, *3*, 020–033.
35. Du, L.; Zhai, K.; Li, X.; Liu, S.; Tao, Y. Ultrasonic Vibration Used for Improving Interfacial Adhesion Strength between Metal Substrate and High-Aspect-Ratio Thick SU-8 Photoresist Mould. *Ultrasonics* **2020**, *103*, 106100, doi:10.1016/j.ultras.2020.106100.

 doi:10.20944/preprints202212.0074.v1

36. Kérourédan, O.; Rémy, M.; Oliveira, H.; Guillemot, F.; Devillard, R. Laser-Assisted Bioprinting of Cells for Tissue Engineering. In *Laser Printing of Functional Materials*; John Wiley & Sons, Ltd, 2018; pp. 349–373 ISBN 978-3-527-80510-5.
37. Mackay, B.S.; Praeger, M.; Grant-Jacob, J.A.; Kanczler, J.; Eason, R.W.; Oreffo, R.O.C.; Mills, B. Modeling Adult Skeletal Stem Cell Response to Laser-Machined Topographies through Deep Learning. *Tissue and Cell* **2020**, *67*, 101442, doi:10.1016/j.tice.2020.101442.